Isolation and characterization of human monoclonal antibodies to pneumococcal capsular polysaccharide 3.

Rachelle Babb [a], Christopher R Doyle [b] & Liise-anne Pirofski [a]#.

[a] Division of Infectious Diseases, Department of Medicine, Albert Einstein College of Medicine & Montefiore Medical Center, Bronx, New York, USA.

[b] WCG IBC Services, Puyallup, Washington, USA.

Running Title: Pneumococcal human monoclonal antibodies

Address correspondence to Liise-anne Pirofski, MD

Address: 1300 Morris Park Avenue, Bronx, NY, 10461

Phone: 718-430-2940, Fax: 718-430-8968

Email: l.pirofski@einsteinmed.org

Word count

Abstract: 223 words

Importance: 144 words

Text: 4444 words

ABSTRACT:

The current pneumococcal capsular polysaccharide (PPS) conjugate vaccine (PCV13) is less effective against *Streptococcus pneumoniae* serotype 3 (ST3), which remains a major cause of pneumococcal disease and mortality. Therefore, dissecting structure-function relationships of human PPS3 antibodies may reveal characteristics of protective antibodies. Using flow cytometry, we isolated PPS3-binding memory B cells from pneumococcal vaccine recipients and generated seven human PPS3-specific monoclonal antibodies (humAbs). Five humAbs displayed ST3 opsonophagocytic activity, four induced ST3 agglutination *in vit*ro, and four mediated both activities. For two humAbs, C10 and C27, that used the same variable heavy (V_H) and light (V_L) chain domains (V_H3-9*01/V_L2-14*03), C10 had fewer V_L somatic mutations, higher PPS3 affinity, more ST3 opsonophagocytic and agglutinating activity, whilst both humAbs altered ST3 gene expression *in vitro*. After V_L swaps, C10V_H/C27V_L exhibited reduced ST3 binding and agglutination, but C27V_H/C10V_L binding was unchanged. In C57Bl/6 mice, C10 and C27 reduced nasopharyngeal colonization with ST3 A66 and a clinical strain, B2, and prolonged survival following lethal A66 intraperitoneal infection, but only C10 protected against lethal intranasal infection with the clinical strain. Our findings, associate efficacy of PPS3-specific humAbs with ST3 agglutination and opsonophagocytic activity and reveal an unexpected role for the V_L in functional activity *in vitro* and *in vivo*. These findings also provide insights that may inform antibody-based therapy and identification of surrogates of vaccine efficacy against ST3.

47 **IMPORTANCE:**

48 Despite the global success of pneumococcal conjugate vaccination, serotype 3 (ST3)
49 pneumococcus remains a leading cause of morbidity and mortality. In comparison to other
50 vaccine-included serotypes, the ST3 pneumococcal capsular polysaccharide (PPS3) induces a
51 weaker opsonophagocytic response, which is considered a correlate of vaccine efficacy. Previous
52 studies of mouse PPS3 monoclonal antibodies identified ST3 agglutination as a correlate of
53 reduced ST3 nasopharyngeal colonization in mice, however neither the agglutinating ability of
54 human vaccine-elicited PPS3 antibodies nor their ability to prevent experimental murine
55 nasopharyngeal colonization has been studied. We generated and analysed the functional and *in*
56 *vivo* efficacy of human vaccine-elicited PPS3 monoclonal antibodies and found that ST3
57 agglutination associated with antibody affinity, protection *in vivo*, and limited somatic mutations
58 in the light chain variable region. These findings provide new insights that may inform the
59 development of antibody-based therapies and next generation vaccines for ST3.

60

61

62

63

64

65

66

67

INTRODUCTION:

The current pneumococcal capsular polysaccharide conjugate vaccine, PCV13 is less effective against *S. pneumoniae* serotype 3 (ST3) than other vaccine-included serotypes (ST)'s. As a result, ST3 is a major cause of pneumonia and mortality in adults and children (1-5). Ample clinical data show that efficacy of pneumococcal conjugate vaccination reflects vaccine-mediated prevention of pneumococcal colonization and transmission, with vaccine-elicited ST-specific opsonophagocytic serum antibodies generally considered a surrogate for vaccine efficacy (6-8). However, a relationship between vaccine-elicited opsonophagocytic antibodies and protection against ST3 has not been established. In addition, compared to other vaccine-included STs, the capsular polysaccharide of ST3 (PPS3) is poorly immunogenic and induces a weaker opsonophagocytic antibody response (2). This reduced immunogenicity has been attributed to the thick ST3 capsule (9) as well as the limited ability of PPS3 antibodies to clear ST3 via opsonophagocytosis *in vivo* due to large amounts of ST3 capsule shedding (10). Nevertheless, opsonophagocytic PPS3 mouse and human monoclonal antibodies (mAbs) that are protective in ST3 sepsis and pneumonia models in mice have been generated (11-15). Notably, an opsonophagocytic mAb that protected against ST3 sepsis and pneumonia did not reduce ST3 colonization, whereas a non-opsonic mAb that agglutinated ST3, reduced colonization, protected against sepsis and pneumonia and also altered ST3 gene expression *in vitro* and *in vivo* (11, 13, 16).

Bacterial agglutination, including that of the pneumococcus, is a long-recognized correlate of PPS antibody efficacy in experimental models (17, 18). Whilst mouse and human PPS3 mAbs elicited by an experimental PPS3-TT conjugate revealed that ST3 opsonophagocytosis and

agglutination were mutually exclusive functions (11, 13, 16, 19), serum derived antibodies to ST4 and ST23 exhibited both opsonophagocytic and agglutinating functions (20). Consistent with the latter, among a set of 5 PPS3 mouse mAbs generated in response to a PPS3-KLH conjugate, 4 exhibited both opsonophagocytic and agglutinating activity and only one mediated opsonophagocytosis (21). These findings suggest that the nature of PPS3 antibodies that mediate opsonophagocytosis and agglutination versus those that mediate one function and not the other may differ.

Reduced efficacy of PPS3-specific antibodies against ST3 disease has been attributed to impaired opsonophagocytic clearance, and it has been estimated that approximately 8 times more antibody is required to confer protection against ST3 based on the calculated correlate of protection for other pneumococcal STs (2, 10). Thus, deciphering the structural and functional characteristics of human vaccine elicited PPS3 antibodies may advance understanding of vaccine failure and facilitate development of antibody-based therapies and next generation vaccines. To gain insight into the nature of human PPS3-binding antibodies, we generated PPS3 human mAbs (humAbs) from human pneumococcal vaccine recipients and determined their molecular derivation, PPS3 binding, and function *in vitro* and *in vivo*.

RESULTS:

PPS3 humAbs use gene segments from the VH3 family.

Seven PPS3-binding humAbs (PPS3 humAbs) were generated and tested for PPS3 binding by ELISA (Figure 1). C38 had the strongest binding to PPS3 (EC_{50}= 0.09 μg/ml), followed by C34 (EC_{50}= 0.21 μg/ml), and C10 (EC_{50}= 0.24 μg/ml). Binding to a ST3 clinical strain, B2 was also

similar by whole cell ELISA and immunofluorescence (Figure S1 & S2).

Sequencing analysis revealed that five humAbs (C10, C12, C27, C34, C38) used lambda light chains (LC)s and two (C11, C18) used kappa LCs. Based on IgBlast, six used variable heavy 3 (V_H3) genes and one (C38) used a V_H1 gene (Table 1). All seven humAbs had V_H and V_L CDR as well as FR somatic mutations (Figure S3 & S4). In addition, all seven humAb CDR3s differed by sequence and length, but four (C10, C27, C38, C11) had an Ala-Arg-Asp: ARD or Ala-Arg-Gly: ARG motif at the beginning of the V_H CDR3 region (Table 1). Two lambda humAbs, C10, C27 used the same heavy VDJ and LC VJ segments, but their FRs and CDRs differed by several somatic mutations (Figure 2). C10 and C27 had respectively, 9 and 8 V_H mutations conferring amino acid changes relative to germline IGHV3-9*01, including 4 at the same positions and a shared Lysine (K) in CDR2. C10 V_L was closer to germline IGVL2-14*03, with fewer mutations (5 versus 11) than C27, 4 of which were shared.

PPS3 humAbs agglutinate ST3 *in vitro*.

It has been previously reported that antibodies that agglutinate pneumococcus can reduce pneumococcal colonization (13, 22, 23). Thus, we determined the ability of the PPS3 humAbs to agglutinate ST3 A66 and the clinical strain, B2 by flow cytometry and validated our findings with light microscopy. C10, C12, C34 and C38 each exhibited dose-dependent agglutination of ST3. At 10 µg/ml, C34 and C38 agglutinated ~75% and 89% of bacteria, respectively, whilst C10 and C12 agglutinated ~48% and 39%, respectively (Figure 3A & B). Visual ST3 clumping was also observed with C10, C12, C34 and C38 by light microscopy (Figure 3C). Similar results regarding agglutination experiments were obtained with the clinical strain, B2 (Figure S5). $F(ab')_2$ fragments of C10 and C38 also agglutinated ST3 with levels comparable to their

respective whole IgG (Figure 4A & B).

Opsonophagocytosis of ST3 by PPS3 humAbs.

Functional activity of the humAbs was determined with the standard opsonophagocytic assay (OPA) used in the field (24, 25). C10 and C38 displayed the highest activity with significant reductions in CFU at 0.74 μg/ml (Figure 5) relative to the IgG1 control. C12, C18 and C34 reduced CFU at 2.2 μg/ml, and C11 and C27 at 20 μg/ml. When humAbs were incubated with ST3 without HL60 cells, C10, C18, C27, C34 and C38 reduced CFU relative to the control. This correlated with agglutination, except for C27.

PPS3 humAbs reduce A66 and B2 nasopharyngeal colonization in C57Bl/6 mice.

We next performed nasopharyngeal (NP) colonization experiments in mice with C10 and C27. These humAbs were used because they use the same V_H3-9*01/V_L2-14*03 gene elements but have different affinities and functional activity *in vitro*. Compared to the IgG1 control, administration of C10 and C27 reduced NP CFU after infection with A66 (C10; P=0.0388, C27; P=0.0437) (Figure 6A) and B2 (C10; P=0.0128, C27; P=0.0015) (Figure 6B). CFU were not detected in the lungs (data not shown). Compared to IgG1-treated controls, B2-infected C10- and C27-treated mice had significantly lower TNF-α, IL-1α and IL-6 levels 4 days post infection (Figure 6C).

PPS3 humAbs prolong survival of mice lethally infected with A66 and B2.

The efficacy of C10, C27, and C38 was next investigated in lethal ST3 infection models. C38 was included because it exhibited strong ST3 binding, opsonophagocytosis, and agglutination. IP

160 administration of all three mAbs prolonged survival after IP infection with A66 (Figure 7A). C10
161 was the most protective (92% survival, P=0.0001), followed by C27 (76%, P=0.001), and C38
162 (70%, P=0.0036). In a lethal IN infection model, IN administration of C10, but not C27
163 prolonged survival after infection with B2 (85%, P=0.0291) compared to the IgG1 control
164 (Figure 7B).
165
166 **HumAbs alter bacterial gene expression *in vitro*.**
167 Given that C27 did not promote agglutination or opsonophagocytosis *in vitro*, yet it reduced
168 colonization and protected against lethal IP infection (sepsis), we sought an alternative
169 mechanism by which it could mediate protection. Previous work showed that defined PPS3
170 mAbs enhanced ST3 A66 transformation frequency and competence, and one mAb, 1E2, altered
171 ST3 gene expression *in vitro* and *in vivo* (13, 16, 19). Thus, we performed RT-qPCR on reactions
172 of ST3 A66 incubated with C10 and C27 to analyze expression of ST3 genes that induce or
173 respond to oxidative stress (*dpr*, *piuB*, *blpX*, *merR*, *comX*) and of which expression was altered in
174 1E2-treated mice following NP colonization (16). In comparison to an IgG1 control, C10 and
175 C27 each induced a significant decrease in *dpr* gene expression (Figure 8). We also observed a
176 decrease in *piuB*, *blpX*, *merR* and *comX* expression (Figure 8). There were no significant
177 differences between C10 and C27 in the genes examined.
178
179 **Analysis of humAbs with V_L swaps.**
180 Given that C10 and C27 use the same V_H and V_L, but C27 had lower affinity, reduced ST3
181 binding and more mutations in its V_L region relative to the germline, we performed V_L swaps to
182 evaluate the effect of V_L on binding and agglutination. PPS3 and B2 binding of C10 expressing

183 the V_L of C27 ($C10_HC27_L$) was reduced compared to that of native C10, whereas C27 exhibited
184 no differences in binding when expressing the C10 V_L ($C27_HC10_L$) (Figure 9A). In agglutination
185 experiments with B2, 20 μg/ml of C10 promoted strong agglutination (~75%) compared to
186 $C10_HC27_L$ (~10%), but there were no differences in agglutination for $C27_HC10_L$ relative to native
187 C27 (Figure 9B & C).
188
189 **DISCUSSION:**
190 Here we report the gene use and *in vitro* functional activity of seven PPS3 humAbs generated
191 from pneumococcal vaccine recipients. We also demonstrate the efficacy of two humAbs (C10 &
192 C27) which use the same V_H and V_L genes (V_H3-9*01/V_L2-14*03) against NP colonization and
193 lethal ST3 infection in mice. Our data show that the humAbs with the highest affinity, C10, C34,
194 and C38, mediated the most ST3 agglutination and opsonophagocytic activity. Agglutinating
195 PPS antibodies have been reported to enhance complement activation and complement-
196 dependent killing *in vitro* and have also been shown to be important for reducing pneumococcal
197 colonization in mice (20, 22, 23). Notably in our study, humAb ST3 agglutination occurred at
198 low concentrations (≤20 μg/ml), whereas other reported PPS antibodies mediated agglutination
199 of ST14 (100 μg/ml) (22) and ST23 (250 μg/ml) (23) at much higher concentrations. It is
200 possible that humAb agglutination could have augmented CFU reductions in the OPA, as this
201 was observed in the absence of HL60 cells. However, we do not know if this reflected ST3
202 clumping or killing (26).
203
204 Consistent with prior work demonstrating V_H3 restriction of PPS- and other polysaccharide-
205 binding antibodies (27-30), each humAb except C38 used a V_H3 gene element. PPS3-specific

206 residues important for PPS23F binding of a V_H3-30 humAb (31) were not present in our humAbs.
207 However, C10, C27, C38, C11, each had Ala-Arg-Asp: ARD or Ala-Arg-Gly: ARG V_H CDR3
208 motifs, which have been described in PPS-binding (32) and polyreactive antibodies from
209 pneumococcal vaccine recipients (33). There were no common V_L motifs, but the C18 V_L CDR3
210 was identical to a PPS8-binding kappa humAb that used the same V_L gene (V_L 2-30) (32).
211 Serological cross reactivity has not been described for PPS3 and PPS8, but they are similar
212 structurally (34).
213
214 In depth analysis of C10 and C27 humAbs revealed that in contrast to C10, C27 had lower PPS3
215 affinity, minimal agglutinating ability, did not mediate opsonophagocytosis and had more
216 somatic mutations in its V_L relative to the germline. Nonetheless, both C10 and C27 reduced NP
217 colonization with ST3 A66 and the clinical ST3 strain, B2 (Table 2). Similarly, both humAbs
218 prolonged survival after lethal A66 IP infection, suggesting that complement and neutrophils in
219 the blood may have enhanced the ability of lower affinity C27 to mediate ST3 clearance, as
220 described for polyclonal IgG (35). However, IN administration of C10, but not C27 was
221 protective against lethal IN challenge with B2. Even though both humAbs reduced NP
222 colonization and inflammatory cytokines in the NP colonization model with this strain, it appears
223 that only C10 prevented dissemination. Notably, an agglutinating mouse mAb, 1E2, prevented
224 dissemination to the lungs after NP colonization, whereas an opsonic mouse mAb, 7A9, did not
225 (13). However, we do not know if the reduced efficacy of C27 in this model reflects an inability
226 to prevent dissemination, and/or distinct features of the ST3 clinical strain, B2. Tissue specific
227 differences in virulence have been identified for other STs (36, 37), but further work is needed to
228 dissect the roles that humAbs and ST3 strain specific differences may play in the reduced

229 efficacy of C27 observed in the lethal IN infection model.

230

231 The main mechanism by which pneumococcal vaccine-elicited antibodies are thought to confer
232 protection is by mediating ST-specific opsonophagocytosis and this function has been considered
233 a surrogate for vaccine efficacy in clinical studies (6-8). While vaccine effectiveness studies
234 support this association for most vaccine-included STs, this is not the case for ST3 (against
235 which current vaccines are less effective compared to other STs) (2). Given that our data show
236 that C10, which was highly agglutinating and opsonophagocytic, reduced colonization and
237 protected against lethal ST3 infection, its efficacy could stem from its agglutinating ability.
238 There is now ample evidence that ST-specific agglutination can reduce NP colonization in mice
239 (13), but less evidence that opsonophagocytic antibodies reduce colonization. In fact, a PPS
240 mouse mAb (7A9) protected against pneumonia and sepsis but did not reduce colonization in
241 mice (11, 13). Thus, it is possible that ST-specific agglutination, which has not been examined as
242 a correlate of pneumococcal vaccine efficacy in clinical studies, may be a better correlate of
243 vaccine effectiveness against pneumococcal colonization and transmission than
244 opsonophagocytosis. In support of this concept and previously highlighted, agglutinating PPS
245 antibodies are important in prevention of pneumococcal colonization in mice (20, 22, 23). While
246 this may help explain how C10 and C38 worked in our models, it does not explain the efficacy of
247 C27.

248

249 Given that C27 did not exhibit agglutination or opsonophagocytosis *in vitro*, but reduced
250 colonization and prevented death from IP infection *in vivo*, it may have mediated these functions
251 *in vivo*. Nevertheless, its lower affinity seems to make this unlikely and we cannot explain its

activity based on known mechanisms of PPS antibody action. Thus, we explored the possibility that both C10 and C27 may exert direct effects on ST3 and alter its biological state, as described for a mouse PPS3 mAb that altered gene expression and affected ST3 survival (16, 19). Similarly, we observed a downregulation in *dpr,* which is normally expressed in response to intracellular iron and needed to sequester iron to protect bacteria from oxidative damage (38-40). However, in contrast to the previous *in vivo* study, our *in vitro* data show that C10 and C27 reduced expression of other ST3 genes including *blpX*, an immunity gene needed to avoid bacteriocin-mediated suicide and protect against other bacteriocins (41) and *piuB*, which is essential for regulating iron transport (42). Given their importance in the response to oxidative stress, it is possible that PPS3 antibody-mediated downregulation of these genes could affect ST3 survival. In fact, alteration of ST2 pneumococcal gene expression was reported with penicillin treatment, which similarly reduced expression of genes related to pneumococcal iron uptake (Piu) operon *piuBCDA* and competence (43). Experiments to assess the effect of these humAb-induced changes in ST3 gene expression *in vitro* on ST3 viability *in vivo* are beyond the scope of the current study.

The affinity differences between C10 and C27 could be related to their distinct V_H and V_L mutations. Notably, for clonally related PPS14 Fabs, the more extensively mutated V_H region had lower affinity (44). Similarly, more highly mutated mouse *Cryptococcus neoformans* capsular polysaccharide mAbs had lower affinity and less efficacy *in vivo* (45). Although C10 and C27 have a comparable number of mostly distinct V_H mutations, the C10 V_L (IGVL2-14*-03) is closer to germline than C27. Given that the C10 LC swap ($C10_HC27_L$) had lower PPS3 affinity and was less agglutinating than native C10, its superior binding and efficacy against B2

may depend on its V_L structure. Notably, structure-function studies of viral antibodies have revealed that V_L gene use and structure can dictate whether an antibody is neutralizing or non-neutralizing (46, 47). Our data show that the C10 V_L plays a critical role in its agglutinating activity, which was lost when we substituted its V_L with the V_L of C27. On the other hand, substituting the C27 V_L with that of C10 did not alter its agglutinating activity. Together, these findings highlight the potential importance of V_L structure and V_H/V_L pairing for PPS3 agglutination, which may depend on a specific PPS3 epitope-humAb interaction. Understanding this interaction will require identification of humAb PPS3 epitopes and structural requirements for binding, as recently reported for a PPS3 mouse mAb V_H (21) however with a focus on the V_L.

To our knowledge, this is the first in depth report of the binding and functional characteristics of pneumococcal vaccine elicited PPS3 humAbs. Our findings reveal an unexpected role for the V_L in PPS3 binding and agglutination, and confirm prior reports demonstrating the ability of PPS3 antibodies to affect ST3 gene expression *in vitro*, suggesting a possible mechanism by which non-opsonic and non-agglutinating antibody functions may translate into an ability of certain human PPS3 antibodies to reduce ST3 NP colonization. Although more extensive analyses are needed to understand the impact of PPS3-humAb structure-function relationships on antibody-mediated protection, our data suggest that such investigations will be needed to inform the development of therapeutic ST3 humAbs and more immunogenic ST3 vaccines, which remain urgently needed given the continued threat of ST3 infection globally (1-5).

MATERIALS & METHODS:

Bacteria

S. pneumoniae ST3 strain A66 (provided by David Briles; University of Alabama at Birmingham, AL) and a clinical ST3 strain, B2 (isolated in the Montefiore Medical Center (MMC) clinical microbiology laboratory under Albert Einstein College of Medicine IRB protocol 2014-4035) were grown as previously described (13).

Mice

6-8 week-old wildtype (WT) female C57BL/6 mice (NCI) were housed in the Albert Einstein College of Medicine Institute for Animal Studies (IAS). All animal studies were approved by the Institutional Animal Care and Use Committee at Albert Einstein College of Medicine (protocol #20171212).

PBMC blood collection

After obtaining informed consent under Einstein/Montefiore Institutional Review Board protocol 2016-7376, PBMCs were isolated by density gradient centrifugation as described (48) from whole blood of healthy volunteers seven days after pneumococcal vaccination (Pneumovax or Prevnar13). PBMCs were stored in liquid nitrogen prior to use.

PPS3-PE antigen optimization

Concentrations of fluorescently conjugated PPS3 (PPS3-PE) (Fina BioSolutions) were incubated with ST3 mouse hybridoma cells (11) with or without unlabelled PPS3 (25 μg/well). PPS3-PE

positive cells were gated by flow cytometry with cells without PPS3-PE as negative controls. The optimal concentration had similar background fluorescence to control cells (Figure S6).

Sorting of PPS3-binding memory B cells by flow cytometry

PBMCs were combined from 3 pneumococcal vaccine recipients (two Pneumovax and one PCV13 recipient), to increase probability of isolating PPS3-specific memory B cells. PPS3-memory B cells were defined as ($CD19^+CD27^+IgM^-IgG^+PPS3^+$). PBMCS were stained with PPS3-PE and anti-human fluorescently-conjugated: CD19-PE-Cy7, CD27-APC, IgM-FITC, IgG-V421, CD3-V500, CD4-V500, CD8-V500 and CD14-V500 (BD). Live/dead (LD) cells were identified with Zombie aqua fixable viability kit (Biolegend). CD3, CD4, CD8 and CD14 positive cells were excluded. Gating strategy shown in Figure S7. Single cells were sorted on a BD FACSAria II into 96-well PCR plates (MicroAmp Endura Optical 96-Well Clear Reaction Plates, Life technologies) into lysis buffer as described (49).

HumAb generation

Variable heavy (V_H) and light (V_L) chain immunoglobulin genes from sorted B cells were PCR amplified, sequenced, cloned, and produced as human IgG1s in HEK-293 cells as described (49, 50). For cloning and ligation into human IgG1 expression vectors (IgG-AbVec (PBR322 based), Igκ-AbVec (PBR322 based) and Igλ-AbVec (PBR322 based) (obtained from (50)), refined primers listed in (51) were used to generate DNA fragments with overlapping ends. Gibson assembly was performed to ligate DNA fragments with their corresponding digested vectors using the NEBuilder® HiFi DNA Assembly Master Mix (NEB) according to the manufacturer's guidelines. Sequencing of V_H and V_L regions was performed by GENEWIZ (New Jersey, NY).

343 HumAbs were purified using the Gentle Ag/Ab binding and Elution Buffer kit (Thermo
344 Scientific). HumAbs were concentrated using Millipore amicon ultra centrifugal filter tubes (30K
345 MWCO) and resuspended in 200mM NaCl and 20mM Hepes pH 7.4.
346
347 **ELISA to determine binding profiles**
348 PPS3 ELISAs were performed using 96-well Nunc Maxisorp plates (Thermofisher Scientific)
349 coated with purified PPS3 (ATCC) (10 µg/ml) in PBS overnight at 4°C as described (11, 52).
350 Pneumococcal polysaccharide 8 (PPS8) (ATCC) (10 µg/ml) was used as a negative control. The
351 numerical half-maximal binding titer (EC_{50}) was determined by graphpad prism. A whole-cell
352 ELISA (53) was used to determining binding to the clinical strain B2, similar for PPS3.
353
354 **Generation of F(ab')$_2$ fragments**
355 F(ab')$_2$ fragments were generated using IdeZ protease (NEB), purified using CaptureSelect LC-
356 lambda affinity matrix (human) (ThermoFisher), and concentrated with amicon ultra centrifugal
357 filter tubes (30K MWCO) according to manufacturers' instructions. Digestion and purification
358 were confirmed by SDS-PAGE using mini-PROTEAN TGX pre-cast gels (4-20%) (BioRad).
359
360 ***In vitro* agglutination of ST3 bacteria**
361 HumAb agglutination of ST3 was determined by flow cytometry as described (23, 54). ST3
362 strains A66 or B2 (1x 10^5 CFU) were incubated with humAbs, F(ab')$_2$ fragments or human IgG1
363 (control) (Southern Biotech) for 1hr at 37°C in a 96-well plate. Cells were fixed with 1%
364 paraformaldehyde and analysed by flow cytometry. Bacteria were gated on forward (FSC) and
365 sideward (SSC) scatter (referring to cell size and granularity) to determine percentage

366 agglutination. Agglutination was also assessed by light microscopy. Aliquots from each sample
367 were spotted onto 1% agarose pads and visualized with an AxioImager Z1 microscope (Zeiss).
368
369 **Immunofluorescence**
370 HumAbs (20 µg/ml) were mixed with $1x10^6$ bacteria (50ul) in microcentrifuge tubes and
371 incubated for 1hr at 37°C. Bacteria were washed 1x with PBS by centrifugation and anti-human
372 IgG-FITC was added to each sample and incubated for 1hr at 37°C. After washing, aliquots
373 were spotted onto 1% agarose pads and visualized with an AxioImager Z1 microscope (Zeiss)
374 (100X magnification).
375
376 **Opsonophagocytosis assay (OPA)**
377 The assay was performed with differentiated HL-60 cells at an effector/target cell ratio of 400:1
378 as described (11, 24). HumAbs and IgG1 (control) (Southern Biotech) were diluted 3-fold from
379 20 µg/ml. ST3 (A66) killing (%) was determined in the presence of humAbs under 2 conditions:
380 with HL60 cells and complement (3-4 week rabbit complement, Pel-Freez) or without HL60
381 cells (humAbs and bacteria only), by plating aliquots of samples onto blood agar plates and
382 enumerating CFU.
383
384 ***In vitro* bacterial gene expression by reverse transcription-quantitative PCR (RT-qPCR).**
385 To analyse the expression of selected genes during *in vitro* growth as previously described (16),
386 in brief bacteria were grown as described above, diluted to a starting OD of ~0.01 and 1 ml of
387 culture was incubated with humAbs (C10, C27) or IgG1 control at a concentration of 10 µg/ml
388 for 1.5 hours at 37ºC. Bacterial RNA was extracted using the TRIzol Max Bacterial RNA
389 isolation kit (Life technologies) using the manufacturers protocol. RNA was then Dnase treated

using the TURBO DNA free kit (Invitrogen) and cDNA was synthesized from 200 ng RNA using the iScript cDNA synthesis kit (BioRad). qPCR was performed using Power SYBR green master mix (Life Technologies) with 10 ng cDNA and 10 µm primers outlined in Table S1 as per manufacturers instructions. Amplification was performed on a StepOne Plus real-time PCR system (Life Technologies) using the following conditions: 95ºC for 10 mins, followed by 40 cycles of 95ºC for 15 seconds and 60ºC for 1 min. Relative expression of genes in humAb treated bacteria was calculated using the threshold cycle ($2\Delta\Delta C_T$) method as described previously (55) using the 16S rRNA gene as an internal control and control IgG1-treated bacteria as the reference.

Mouse infection experiments

Colonization model: Mice were anesthetized with isofluorane and injected intranasally (IN) with 25 µg of humAbs or anti-human IgG1 (Bxcell) (isotype control) diluted in PBS as described (13). 2hrs after humAb administration, mice were infected IN with either $5x10^5$ CFU of A66 or $1x10^7$ CFU of B2 in 10ul. CFU were enumerated in the nasal lavage (NL) and lungs at the times specified (24 hrs or 4 days) after infection as described (13). NL cytokines were determined after concentration using the Legendplex Mouse inflammation panel (13-plex) (Biolegend) as per manufacturer's protocol.

Lethal infection model: Mice were injected either IP or IN with 25 µg humAb or anti-human IgG1 in PBS as described above. 2hr after humAb administration, mice were infected IP with $5x10^5$ CFU A66 (100ul) or IN with $5x10^7$ CFU B2 in 10ul and monitored for survival.

Nucleotide sequence accession numbers

GenBank accession numbers were as follows: C10V_H, MZ054262, C11V_H, MZ054263, C12V_H, MZ054264, C18V_H, MZ054265, C27V_H, MZ054266, C34V_H, MZ054267, C38V_H, MZ054268;

415 $C10V_L$, MZ054269, $C11V_L$, MZ054270, $C12V_L$, MZ054271, $C18V_L$, MZ054272, $C27V_L$,
416 MZ054273, $C34V_L$, MZ054274 and $C38V_L$ MZ054275.
417
418 **Statistical analysis**
419 Data were analysed using a Fisher's exact test (Survival) or a one-way ANOVA for other
420 analyses as indicated in the figure legends using GraphPad prism. *P*-values ≤0.05 were
421 considered significant.
422
423 **ACKNOWLEDGMENTS:**
424 We thank Phil Gialanella at Montefiore Medical Center for isolation of the clinical strain B2
425 used in the study. This study was supported by the National Institutes of Health grants to LP:
426 R01AG045044 and R01AI123654.
427
428 **AUTHOR CONTRIBUTIONS:**
429 RB designed, performed experiments, analysed, interpreted data and wrote the manuscript. CD
430 assisted with experimental design, contributed to revising and critically reviewing the
431 manuscript. LP supervised the study, designed experiments, interpreted data and wrote the
432 manuscript.
433
434 **DISCLOSURE:**
435 No author has a conflict of interest with the data reported in this article.

REFERENCES:

1. Goettler D, Streng A, Kemmling D, Schoen C, von Kries R, Rose MA, van der Linden M, Liese JG. 2020. Increase in Streptococcus pneumoniae serotype 3 associated parapneumonic pleural effusion/empyema after the introduction of PCV13 in Germany. Vaccine 38:570-577.
2. Andrews NJ, Waight PA, Burbidge P, Pearce E, Roalfe L, Zancolli M, Slack M, Ladhani SN, Miller E, Goldblatt D. 2014. Serotype-specific effectiveness and correlates of protection for the 13-valent pneumococcal conjugate vaccine: a postlicensure indirect cohort study. Lancet Infect Dis 14:839-46.
3. Grabenstein JD, Musey LK. 2014. Differences in serious clinical outcomes of infection caused by specific pneumococcal serotypes among adults. Vaccine 32:2399-405.
4. Wijayasri S, Hillier K, Lim GH, Harris TM, Wilson SE, Deeks SL. 2019. The shifting epidemiology and serotype distribution of invasive pneumococcal disease in Ontario, Canada, 2007-2017. PLoS One 14:e0226353.
5. Groves N, Sheppard CL, Litt D, Rose S, Silva A, Njoku N, Rodrigues S, Amin-Chowdhury Z, Andrews N, Ladhani S, Fry NK. 2019. Evolution of Streptococcus pneumoniae Serotype 3 in England and Wales: A Major Vaccine Evader. Genes (Basel) 10.
6. Romero-Steiner S, Frasch CE, Carlone G, Fleck RA, Goldblatt D, Nahm MH. 2006. Use of opsonophagocytosis for serological evaluation of pneumococcal vaccines. Clin Vaccine Immunol 13:165-9.

7. Henckaerts I, Durant N, De Grave D, Schuerman L, Poolman J. 2007. Validation of a routine opsonophagocytosis assay to predict invasive pneumococcal disease efficacy of conjugate vaccine in children. Vaccine 25:2518-27.

8. Schuerman L, Wysocki J, Tejedor JC, Knuf M, Kim KH, Poolman J. 2011. Prediction of pneumococcal conjugate vaccine effectiveness against invasive pneumococcal disease using opsonophagocytic activity and antibody concentrations determined by enzyme-linked immunosorbent assay with 22F adsorption. Clin Vaccine Immunol 18:2161-7.

9. Hammerschmidt S, Wolff S, Hocke A, Rosseau S, Muller E, Rohde M. 2005. Illustration of pneumococcal polysaccharide capsule during adherence and invasion of epithelial cells. Infect Immun 73:4653-67.

10. Choi EH, Zhang F, Lu YJ, Malley R. 2016. Capsular Polysaccharide (CPS) Release by Serotype 3 Pneumococcal Strains Reduces the Protective Effect of Anti-Type 3 CPS Antibodies. Clin Vaccine Immunol 23:162-7.

11. Tian H, Weber S, Thorkildson P, Kozel TR, Pirofski LA. 2009. Efficacy of opsonic and nonopsonic serotype 3 pneumococcal capsular polysaccharide-specific monoclonal antibodies against intranasal challenge with Streptococcus pneumoniae in mice. Infect Immun 77:1502-13.

12. Weber S, Tian H, van Rooijen N, Pirofski LA. 2012. A serotype 3 pneumococcal capsular polysaccharide-specific monoclonal antibody requires Fcgamma receptor III and macrophages to mediate protection against pneumococcal pneumonia in mice. Infect Immun 80:1314-22.

13. Doyle CR, Pirofski LA. 2016. Reduction of Streptococcus pneumoniae Colonization and Dissemination by a Nonopsonic Capsular Polysaccharide Antibody. MBio 7:e02260-15.

14. Russell ND, Corvalan JR, Gallo ML, Davis CG, Pirofski L. 2000. Production of protective human antipneumococcal antibodies by transgenic mice with human immunoglobulin loci. Infect Immun 68:1820-6.

15. Chang Q, Zhong Z, Lees A, Pekna M, Pirofski L. 2002. Structure-function relationships for human antibodies to pneumococcal capsular polysaccharide from transgenic mice with human immunoglobulin Loci. Infect Immun 70:4977-86.

16. Doyle CR, Moon JY, Daily JP, Wang T, Pirofski LA. 2018. A Capsular Polysaccharide-Specific Antibody Alters Streptococcus pneumoniae Gene Expression during Nasopharyngeal Colonization of Mice. Infect Immun 86.

17. Bull CG. 1915. The Mechanism of the Curative Action of Antipneumococcus Serum. J Exp Med 22:457-64.

18. Bull CG. 1915. The Agglutination of Bacteria in Vivo. J Exp Med 22:484-91.

19. Yano M, Gohil S, Coleman JR, Manix C, Pirofski LA. 2011. Antibodies to Streptococcus pneumoniae capsular polysaccharide enhance pneumococcal quorum sensing. mBio 2.

20. Dalia AB, Weiser JN. 2011. Minimization of bacterial size allows for complement evasion and is overcome by the agglutinating effect of antibody. Cell Host Microbe 10:486-96.

21. Ozdilek A, Huang J, Babb R, Paschall AV, Middleton DR, Duke JA, Pirofski LA, Mousa JJ, Avci FY. 2021. A Structural Model for the Ligand Binding of Pneumococcal Serotype 3 Capsular Polysaccharide-Specific Protective Antibodies. mBio 12:e0080021.

22. Roche AM, Richard AL, Rahkola JT, Janoff EN, Weiser JN. 2015. Antibody blocks acquisition of bacterial colonization through agglutination. Mucosal Immunol 8:176-85.

501 23. Mitsi E, Roche AM, Reine J, Zangari T, Owugha JT, Pennington SH, Gritzfeld JF,
502 Wright AD, Collins AM, van Selm S, de Jonge MI, Gordon SB, Weiser JN, Ferreira DM.
503 2016. Agglutination by anti-capsular polysaccharide antibody is associated with
504 protection against experimental human pneumococcal carriage. Mucosal Immunol
505 doi:10.1038/mi.2016.71.
506 24. Romero-Steiner S, Libutti D, Pais LB, Dykes J, Anderson P, Whitin JC, Keyserling HL,
507 Carlone GM. 1997. Standardization of an opsonophagocytic assay for the measurement
508 of functional antibody activity against Streptococcus pneumoniae using differentiated
509 HL-60 cells. Clin Diagn Lab Immunol 4:415-22.
510 25. Song JY, Moseley MA, Burton RL, Nahm MH. 2013. Pneumococcal vaccine and
511 opsonic pneumococcal antibody. J Infect Chemother 19:412-25.
512 26. Fabrizio K, Manix C, Guimaraes AJ, Nosanchuk JD, Pirofski LA. 2010. Aggregation of
513 Streptococcus pneumoniae by a pneumococcal capsular polysaccharide-specific human
514 monoclonal IgM correlates with antibody efficacy in vivo. Clin Vaccine Immunol
515 17:713-21.
516 27. Maitta RW, Datta K, Lees A, Belouski SS, Pirofski LA. 2004. Immunogenicity and
517 efficacy of Cryptococcus neoformans capsular polysaccharide glucuronoxylomannan
518 peptide mimotope-protein conjugates in human immunoglobulin transgenic mice. Infect
519 Immun 72:196-208.
520 28. Sun Y, Park MK, Kim J, Diamond B, Solomon A, Nahm MH. 1999. Repertoire of human
521 antibodies against the polysaccharide capsule of Streptococcus pneumoniae serotype 6B.
522 Infect Immun 67:1172-9.

523 29. Kolibab K, Smithson SL, Rabquer B, Khuder S, Westerink MA. 2005. Immune response
524 to pneumococcal polysaccharides 4 and 14 in elderly and young adults: analysis of the
525 variable heavy chain repertoire. Infect Immun 73:7465-76.
526 30. Zhou J, Lottenbach KR, Barenkamp SJ, Reason DC. 2004. Somatic hypermutation and
527 diverse immunoglobulin gene usage in the human antibody response to the capsular
528 polysaccharide of Streptococcus pneumoniae Type 6B. Infect Immun 72:3505-14.
529 31. Bryson S, Thomson CA, Risnes LF, Dasgupta S, Smith K, Schrader JW, Pai EF. 2016.
530 Structures of Preferred Human IgV Genes-Based Protective Antibodies Identify How
531 Conserved Residues Contact Diverse Antigens and Assign Source of Specificity to CDR3
532 Loop Variation. J Immunol 196:4723-30.
533 32. Smith K, Muther JJ, Duke AL, McKee E, Zheng NY, Wilson PC, James JA. 2013. Fully
534 human monoclonal antibodies from antibody secreting cells after vaccination with
535 Pneumovax(R)23 are serotype specific and facilitate opsonophagocytosis.
536 Immunobiology 218:745-54.
537 33. Thompson R, Khaskhely, N. , Malhotra, K. , Leggat, D. , Mosakowski, J. , Khuder, S. ,
538 McLean, G. and Westerink, M. . 2012. Isolation and characterization of human
539 polyreactive pneumococcal polysaccharide antibodies. Open Journal of Immunology
540 2:98-110.
541 34. Schumann B, Hahm HS, Parameswarappa SG, Reppe K, Wahlbrink A, Govindan S,
542 Kaplonek P, Pirofski LA, Witzenrath M, Anish C, Pereira CL, Seeberger PH. 2017. A
543 semisynthetic Streptococcus pneumoniae serotype 8 glycoconjugate vaccine. Sci Transl
544 Med 9.

545 35. Reed WP, Stromquist DL, Williams RC, Jr. 1983. Agglutination and phagocytosis of
546 pneumococci by immunoglobulin G antibodies of restricted heterogeneity. J Lab Clin
547 Med 101:847-56.
548 36. Orihuela CJ, Gao G, McGee M, Yu J, Francis KP, Tuomanen E. 2003. Organ-specific
549 models of Streptococcus pneumoniae disease. Scand J Infect Dis 35:647-52.
550 37. Minhas V, Aprianto R, McAllister LJ, Wang H, David SC, McLean KT, Comerford I,
551 McColl SR, Paton JC, Veening JW, Trappetti C. 2020. In vivo dual RNA-seq reveals that
552 neutrophil recruitment underlies differential tissue tropism of Streptococcus pneumoniae.
553 Commun Biol 3:293.
554 38. Hua CZ, Howard A, Malley R, Lu YJ. 2014. Effect of nonheme iron-containing ferritin
555 Dpr in the stress response and virulence of pneumococci. Infect Immun 82:3939-47.
556 39. Yamamoto Y, Poole LB, Hantgan RR, Kamio Y. 2002. An iron-binding protein, Dpr,
557 from Streptococcus mutans prevents iron-dependent hydroxyl radical formation in vitro. J
558 Bacteriol 184:2931-9.
559 40. Tsou CC, Chiang-Ni C, Lin YS, Chuang WJ, Lin MT, Liu CC, Wu JJ. 2008. An iron-
560 binding protein, Dpr, decreases hydrogen peroxide stress and protects Streptococcus
561 pyogenes against multiple stresses. Infect Immun 76:4038-45.
562 41. Bogaardt C, van Tonder AJ, Brueggemann AB. 2015. Genomic analyses of pneumococci
563 reveal a wide diversity of bacteriocins - including pneumocyclicin, a novel circular
564 bacteriocin. BMC Genomics 16:554.
565 42. Brown JS, Gilliland SM, Ruiz-Albert J, Holden DW. 2002. Characterization of pit, a
566 Streptococcus pneumoniae iron uptake ABC transporter. Infect Immun 70:4389-98.

567 43. Rogers PD, Liu TT, Barker KS, Hilliard GM, English BK, Thornton J, Swiatlo E,
568 McDaniel LS. 2007. Gene expression profiling of the response of Streptococcus
569 pneumoniae to penicillin. J Antimicrob Chemother 59:616-26.
570 44. Lucas AH, Moulton KD, Tang VR, Reason DC. 2001. Combinatorial library cloning of
571 human antibodies to Streptococcus pneumoniae capsular polysaccharides: variable region
572 primary structures and evidence for somatic mutation of Fab fragments specific for
573 capsular serotypes 6B, 14, and 23F. Infect Immun 69:853-64.
574 45. Mukherjee J, Nussbaum G, Scharff MD, Casadevall A. 1995. Protective and
575 nonprotective monoclonal antibodies to Cryptococcus neoformans originating from one
576 B cell. J Exp Med 181:405-9.
577 46. Ren J, Nettleship JE, Harris G, Mwangi W, Rhaman N, Grant C, Kotecha A, Fry E,
578 Charleston B, Stuart DI, Hammond J, Owens RJ. 2019. The role of the light chain in the
579 structure and binding activity of two cattle antibodies that neutralize bovine respiratory
580 syncytial virus. Mol Immunol 112:123-130.
581 47. Tzarum N, Giang E, Kadam RU, Chen F, Nagy K, Augestad EH, Velazquez-Moctezuma
582 R, Keck ZY, Hua Y, Stanfield RL, Dreux M, Prentoe J, Foung SKH, Bukh J, Wilson IA,
583 Law M. 2020. An alternate conformation of HCV E2 neutralizing face as an additional
584 vaccine target. Sci Adv 6:eabb5642.
585 48. Zhong Z, Pirofski LA. 1996. Opsonization of Cryptococcus neoformans by human
586 anticryptococcal glucuronoxylomannan antibodies. Infect Immun 64:3446-50.
587 49. Tiller T, Meffre E, Yurasov S, Tsuiji M, Nussenzweig MC, Wardemann H. 2008.
588 Efficient generation of monoclonal antibodies from single human B cells by single cell
589 RT-PCR and expression vector cloning. J Immunol Methods 329:112-24.

50. Smith K, Garman L, Wrammert J, Zheng NY, Capra JD, Ahmed R, Wilson PC. 2009. Rapid generation of fully human monoclonal antibodies specific to a vaccinating antigen. Nat Protoc 4:372-84.

51. Ho IY, Bunker JJ, Erickson SA, Neu KE, Huang M, Cortese M, Pulendran B, Wilson PC. 2016. Refined protocol for generating monoclonal antibodies from single human and murine B cells. J Immunol Methods 438:67-70.

52. Tian H, Groner A, Boes M, Pirofski LA. 2007. Pneumococcal capsular polysaccharide vaccine-mediated protection against serotype 3 Streptococcus pneumoniae in immunodeficient mice. Infect Immun 75:1643-50.

53. Hyams C, Camberlein E, Cohen JM, Bax K, Brown JS. 2010. The Streptococcus pneumoniae capsule inhibits complement activity and neutrophil phagocytosis by multiple mechanisms. Infect Immun 78:704-15.

54. Habets MN, van Selm S, van der Gaast-de Jongh CE, Diavatopoulos DA, de Jonge MI. 2017. A novel flow cytometry-based assay for the quantification of antibody-dependent pneumococcal agglutination. PLoS One 12:e0170884.

55. Pfaffl MW. 2004. Quantification strategies in real-time PCR. AZ of quantitative PCR 1:89-113.

FIGURE LEGENDS:

Figure 1: HumAb binding to pneumococcal polysaccharide 3 (PPS3) by ELISA. Binding as reflected by absorbance at 405 is shown on the Y axis for the humAb concentrations shown on the X axis for each humAb. Results are representative of 3 independent experiments (n = 2). The numerical half-maximal binding titer (EC_{50}) for each humAb is indicated to the right of the panel depicting binding curves of all humAbs.

Figure 2: C10 and C27 variable heavy (V_H) and light (V_L) chain amino acid sequences. HumAb A) V_H and B) V_L sequences aligned with their germline counterparts based on IMGT/V-QUEST (sequence alignment software). Amino acid changes resulting from somatic mutations are indicated within the sequence alignment.

Figure 3: HumAb agglutination of ST3 A66.

The ability of the humAbs to agglutinate ST3 (A66) was assessed by flow cytometry. A) Representative FACS dot plots showing the percentage agglutination of all humAbs and control human IgG1 at various concentrations by flow cytometry B) Percentage of agglutination is shown on the Y axis for different humAb concentrations indicated on the X axis. Graph represents data from 2 independent experiments (n = 2 per condition). C) Light microscopy images of humAbs (20 µg/ml) with ST3 A66. Images at 100x magnification are representative of 3 independent experiments (n = 2). Scale bars, 5 µm. By one-way ANOVA: At 5 µg/ml; (C38 vs IgG1 ***P<0.001), at 10 µg/ml; (C34 & C38 vs IgG1 *P<0.05); at 20 µg/ml (C10, C12, C18, C34 & C38 vs IgG1 **P<0.01), at 40 µg/ml (C10, C12, C18, C27 & C38 vs IgG1 ***P<0.001).

Figure 4: HumAb F(ab)'$_2$ fragment agglutination of ST3 A66.

The ability of whole IgG or F(ab')$_2$ fragments of humAbs (C10, C27, C38) to agglutinate ST3 (A66) was assessed by flow cytometry. A) Representative FACS dot plots showing the percentage agglutination of the indicated whole humAbs, F(ab)'$_2$ fragments, or control IgG1 at various concentrations. B) Bar graph depicting percentage agglutination on the Y axis for whole humAb or F(ab')$_2$ fragment concentrations on the X axis. Results are representative of 2 independent experiments (n = 2 per condition). By one-way ANOVA: At 10 µg/ml; (C38 IgG, C38 F(ab')$_2$ vs their respective IgG1 controls *P<0.05); at 20 µg/ml; (C10 IgG, C10 F(ab')$_2$, C38 IgG, C38 F(ab')$_2$ vs their respective IgG1 controls ***P<0.001); at 40 µg/ml; (C10 IgG, C10 F(ab')$_2$, C38 IgG, C38 F(ab')$_2$ vs their respective IgG1 controls ***P<0.001).

Figure 5: HumAb opsonophagocytic killing of ST3.

HumAbs were tested for their opsonophagocytic killing activity with ST3 (A66) and HL60 cells. Percent killing is shown on the Y axis for the different humAb concentrations shown on the X axis. Results are representative of 2 independent experiments (n = 4 per condition). *P<0.05, **P<0.01, ***P<0.001 (One-way ANOVA) for humAbs vs IgG1 control.

Figure 6: HumAb efficacy against ST3 colonization in C57Bl/6 mice.

HumAbs or a control IgG1 were administered IN in C57Bl/6 mice 2 hrs before IN infection with A) 5 x 10^5 CFU A66 or B) 1 x 10^7 CFU B2. The nasal lavage CFU was enumerated 24 hours (A) or 4 days (B) post infection. CFU are depicted on the Y axis for humAbs shown on the X axis C) Indicated cytokine concentrations via legendplex 4 days after infection of C57Bl/6 mice with 1 x 10^7 CFU B2 (B) are shown on the Y axis for the humAbs on the X axis. Results are

652 representative of 2 independent experiments (n ≥ 5 mice/group). *P<0.05, **P<0.01,
653 ***P<0.001 (One-way ANOVA).
654
655 **Figure 7: HumAb efficacy against lethal challenge with ST3 strains in C57Bl/6 mice.**
656 A) HumAbs or a control IgG1 were administered IP in C57Bl/6 mice 2 hrs before IP infection
657 with 5x 10^5 CFU A66 and then monitored for survival. B) HumAbs or a control IgG1 were
658 administered IN in C57Bl/6 mice 2 hrs before IN infection with 5 x 10^7 CFU B2 and monitored
659 for survival. All curves show percent survival on the Y axis for the indicated humAbs monitored
660 over 14 days shown on the X axis. Results are representative of 2 independent experiments (n ≥
661 7 mice/group). *P<0.05, **P<0.01, ***P<0.001, (Fisher's exact test).
662
663 **Figure 8: HumAbs mediate changes in expression of bacterial genes related to oxidative**
664 **stress *in vitro*.**
665 The fold change in expression of the indicated genes in C10 or C27-treated bacteria relative to
666 the control IgG1-treated bacteria was determined by RT-qPCR at 1.5 hours post-humAb
667 addition. Relative expression of genes was determined using the Pfaffl method (55) (fold change
668 is relative to the IgG1 control treated bacteria, expression =1). Data are pooled from 3
669 independent experiments, 3 samples per condition. *P<0.05, **P<0.01, ***P<0.001, (One-way
670 ANOVA) C10 or C27 vs IgG1.
671
672 **Figure 9: HumAb binding and agglutination of humAbs with light chain swaps.**
673 A) HumAbs (native) with their LC swaps were generated and tested by ELISA for binding
674 reactivity to purified PPS3 and B2. Absorbance at 405 is shown on the Y axis for the humAb

675 concentrations shown on the X axis for each humAb. The numerical half-maximal binding titer
676 (EC_{50}) is depicted on the graph. Results are representative of 3 independent experiments (n = 2).
677 ST3 strain B2 was incubated with increasing concentrations of humAbs (C10, C10 LC swap
678 ($C10_HC27_L$), C27, C27 LC swap ($C27_HC10_L$)) or control IgG1 and analyzed by flow cytometry.
679 B) Representative FACS dot plots showing percentage agglutination of the indicated native
680 humAb or LC swap at various concentrations. C) Line graph depicting percentage agglutination
681 on the Y axis for concentrations of indicated humAbs and LC swaps on the X axis. Results are
682 representative of 2 independent experiments (n = 2 per condition). By one-way ANOVA; at
683 10ug/ml; (C10 vs IgG1, C10 vs C10 LC swap ($C10_HC27_L$) C10 vs C27, C10 vs C27 LC swap
684 ($C27_HC10_L$) ***P<0.001); at 20ug/ml (C10 vs IgG1, C10 vs C10 LC swap ($C10_HC27_L$), C10 vs
685 C27, C10 vs C27 LC swap ($C27_HC10_L$) *P<0.05).
686
687
688
689

TABLES:

Table 1. Heavy and light chain VDJ gene usage and CDR3 sequences for all PPS3 humAbs.

		HEAVY CHAIN				LIGHT CHAIN		
humAb	**LC**	**V gene**	**D gene**	**J gene**	**CDR3**	**V gene**	**J gene**	**CDR3**
C10	λ	IGHV3-9*01	IGHD6-19*01	IGHJ6*04	A R D I E H A V N H P R M M V V	IGLV2-14*03	IGLJ2*01,IGLJ3*01	S S Y T R T N T L V
C27	λ	IGHV3-9*01	IGHD6-19*01	IGHJ6*04	A R D V A H A V N H P R I M S V	IGLV2-14*03	IGLJ2*01,IGLJ3*01,IGLJ3*02	T S Y T T D N T V I
C12	λ	IGHV3-23*04	IGHD6-19*01,IGHD7-27*01	IGHJ4*02	A K R P G D S T G W A F Y F E Y	IGLV4-69*01	IGLJ3*02	Q T W G T G R W V
C34	λ	IGHV3-72*01	IGHD2-8*02,IGHD3-9*01,IGHD6-13*01	IGHJ5*02	A R A T A W S F D P	IGLV2-14*01	IGLJ1*01	S S Y T S T Y I Y V
C38	λ	IGHV1-18*01	IGHD6-13*01	IGHJ4*02	A R G G I T T T G F D Y	IGLV1-51*02	IGLJ3*02	G A W D S S L N A G V
C11	κ	IGHV3-30*03	IGHD3-16*01,IGHD3-16*02	IGHJ4*02	A R G G K G L S G G D Y	IGKV2-28*01	IGKJ1*01	M Q A L Q T P W T
C18	κ	IGHV3-7*01	N/A	IGHJ4*02	G I G R L F Y	IGKV2-30*01	IGKJ2*01	M Q G T H W P Y T

Table 2. Summary of *in vitro* and *in vivo* functions for all PPS3 humAbs.

	In vitro				***In vivo***			
	Binding				**Reduction in Colonization**		**Survival**	
HumAb	**PPS3 EC_{50}**	**ST3 EC_{50}**	**Agglutination**	**OPA**	**A66**	**B2**	**IP → IP Challenge (A66)**	**IN → IN Challenge (B2)**
IgG1 Control	ND	ND	-	-	N	N	8%	14%
C10	0.24	0.51	+	+	Y	Y	92%	85%
C27	2.03	11.0	-	-	Y	Y	76%	29%
C38	0.09	0.05	+	+	N/A	N/A	70%	N/A
C11	19.30	19.20	-	-	N/A	N/A	N/A	N/A
C12	0.55	3.23	+	+	N/A	N/A	N/A	N/A
C18	1.13	2.84	-	+	N/A	N/A	N/A	N/A
C34	0.21	3.01	+	+	N/A	N/A	N/A	N/A

ND = not detected, N/A = not applicable, Y= Yes, N = No, (+) = strong activity, (-) = weak/no activity, IP → IP challenge = Refer to figure 7A, IN → IN challenge = Refer to figure 7B.

FIGURES:

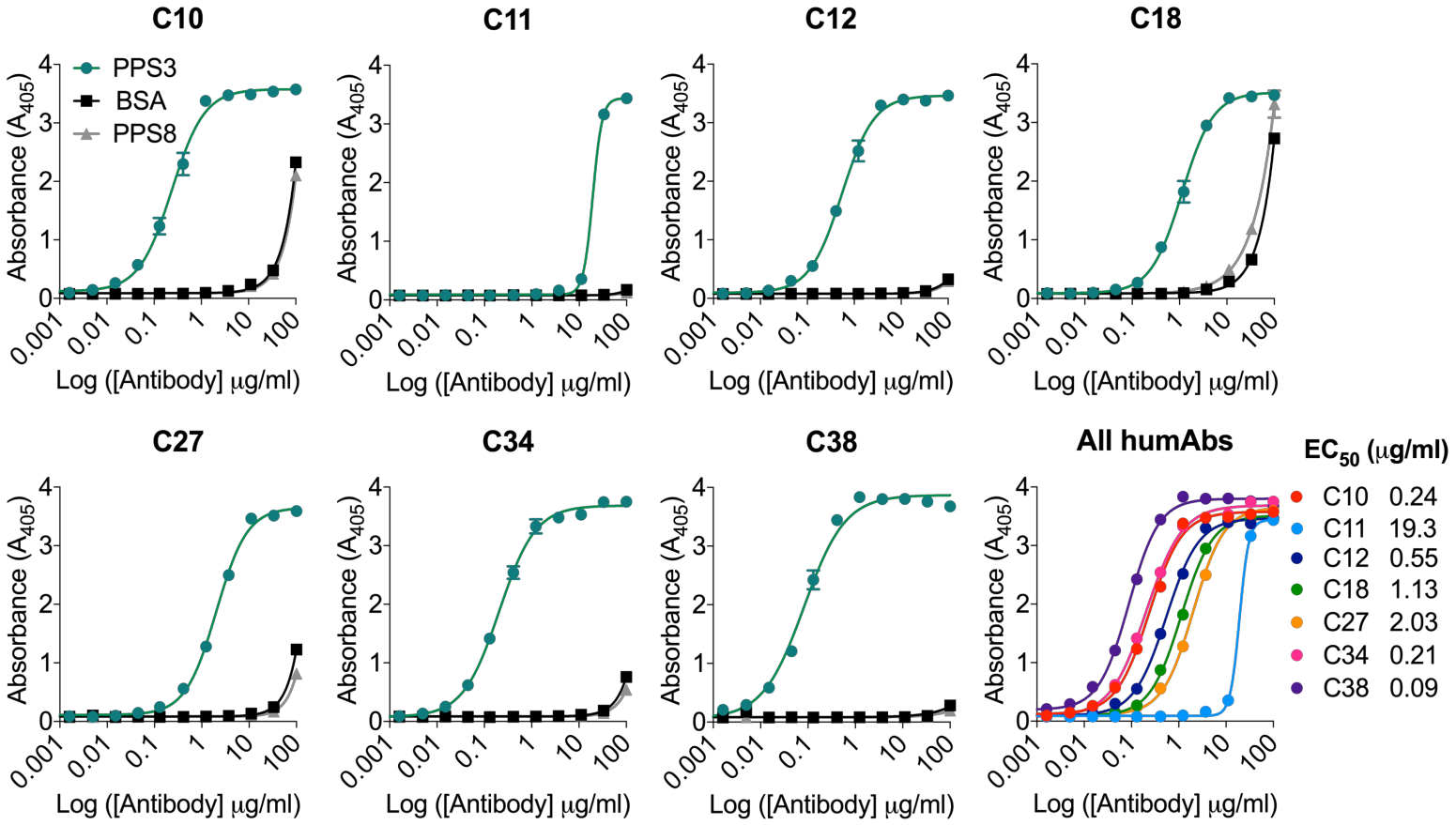

Figure 1: HumAb binding to pneumococcal polysaccharide 3 (PPS3) by ELISA. Binding as reflected by absorbance at 405 is shown on the Y axis for the humAb concentrations shown on the X axis for each humAb. Results are representative of 3 independent experiments (n = 2). The numerical half-maximal binding titer (EC_{50}) for each humAb is indicated to the right of the panel depicting binding curves of all humAbs.

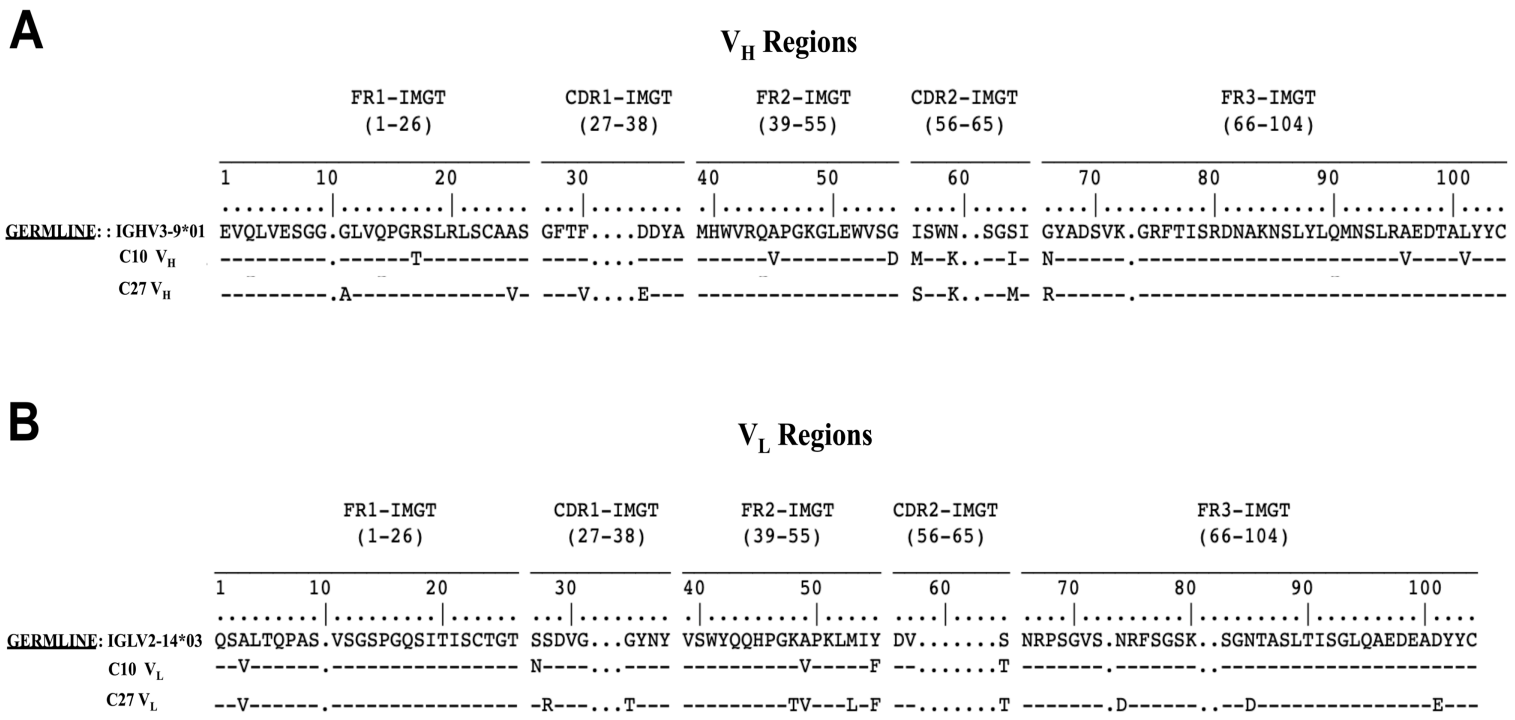

Figure 2: C10 and C27 variable heavy (V_H) and light (V_L) chain amino acid sequences.
HumAb A) V_H and B) V_L sequences aligned with their germline counterparts based on IMGT/V-QUEST (sequence alignment software). Amino acid changes resulting from somatic mutations are indicated within the sequence alignment.

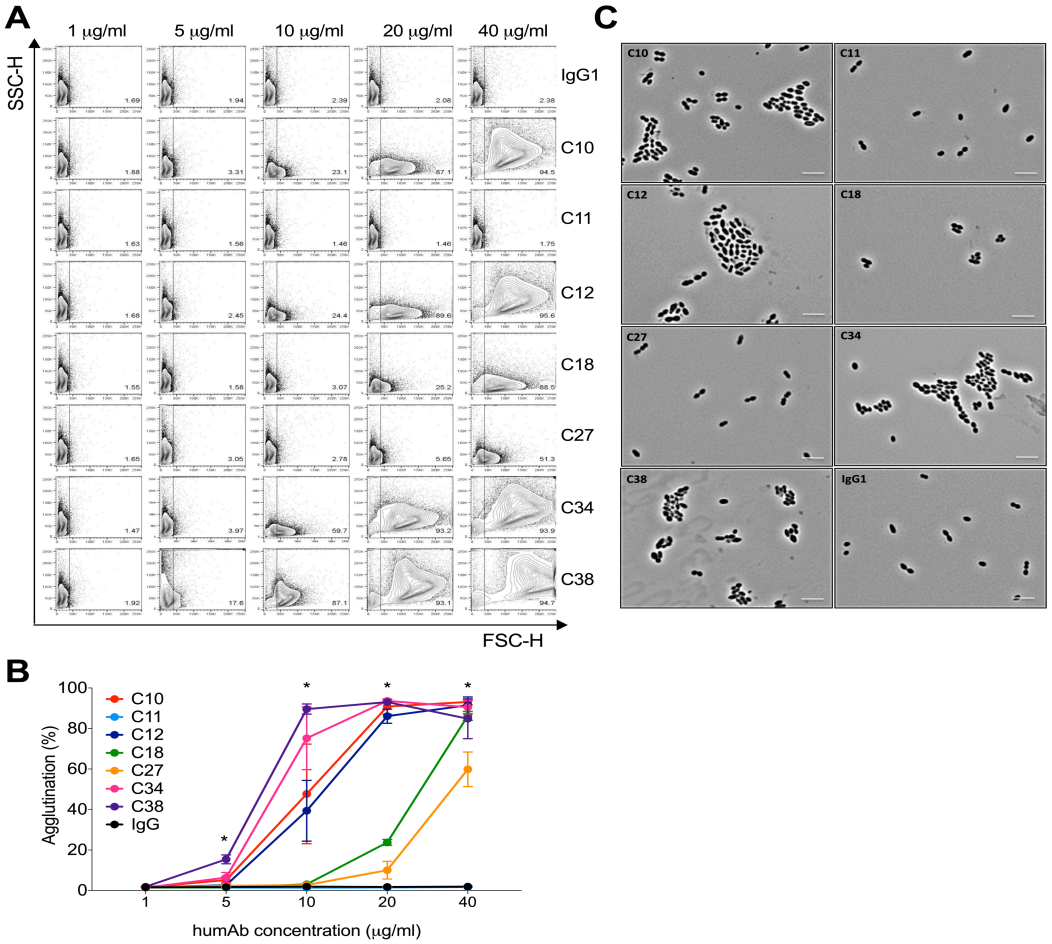

Figure 3: HumAb agglutination of ST3 A66.

The ability of the humAbs to agglutinate ST3 (A66) was assessed by flow cytometry. A) Representative FACS dot plots showing the percentage agglutination of all humAbs and control human IgG1 at various concentrations by flow cytometry B) Percentage of agglutination is shown on the Y axis for different humAb concentrations indicated on the X axis. Graph represents data from 2 independent experiments (n = 2 per condition). C) Light microscopy images of humAbs (20 μg/ml) with ST3 A66. Images at 100x magnification are representative of 3 independent experiments (n = 2). Scale bars, 5 μm. By one-way ANOVA: At 5 μg/ml; (C38 vs IgG1 ***P<0.001), at 10 μg/ml; (C34 & C38 vs IgG1 *P<0.05); at 20 μg/ml (C10, C12, C18, C34 & C38 vs IgG1 **P<0.01), at 40 μg/ml (C10, C12, C18, C27 & C38 vs IgG1 ***P<0.001).

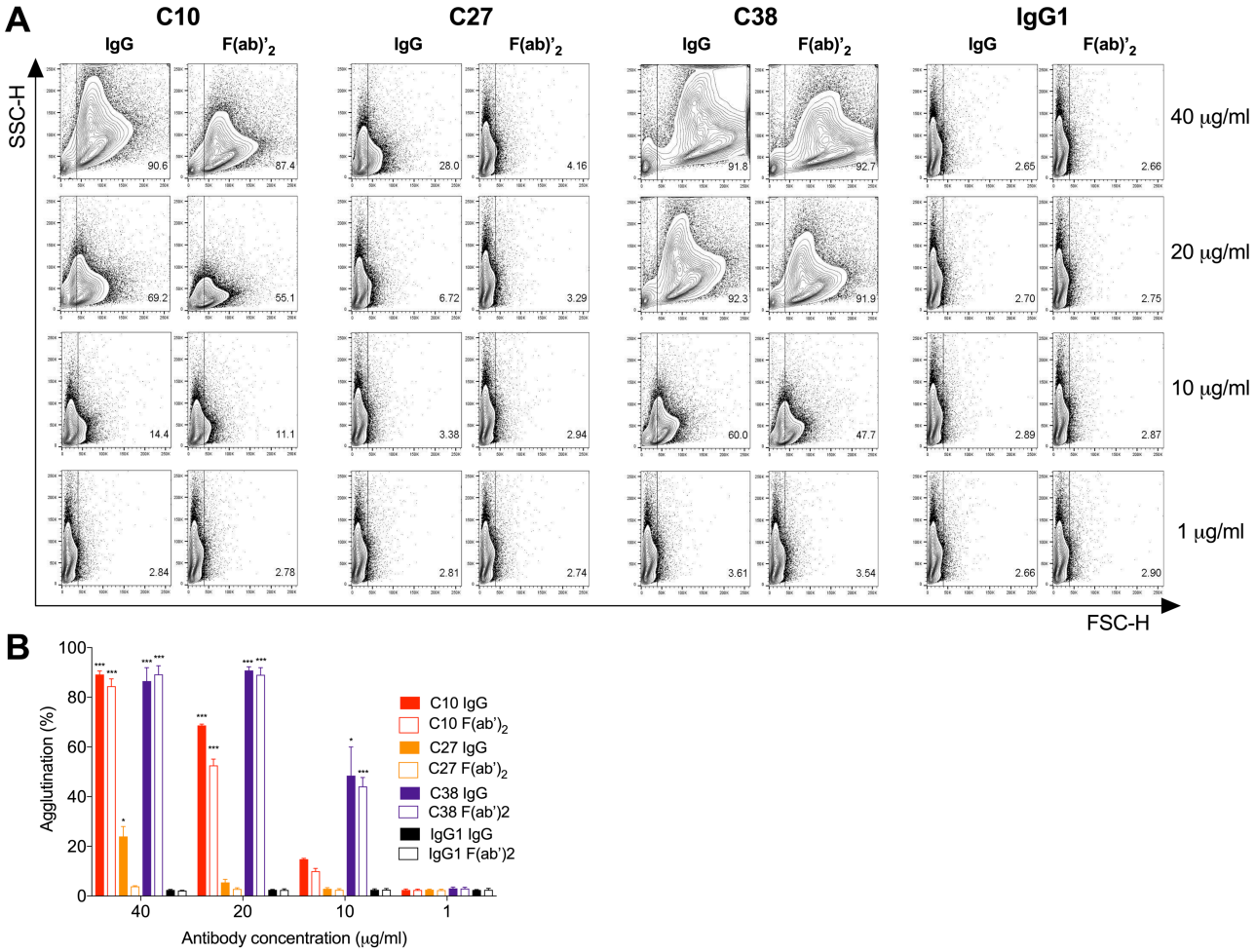

Figure 4: HumAb F(ab)'$_2$ fragment agglutination of ST3 A66.
The ability of whole IgG or F(ab')$_2$ fragments of humAbs (C10, C27, C38) to agglutinate ST3 (A66) was assessed by flow cytometry. A) Representative FACS dot plots showing the percentage agglutination of the indicated whole humAbs, F(ab)'$_2$ fragments, or control IgG1 at various concentrations. B) Bar graph depicting percentage agglutination on the Y axis for whole humAb or F(ab')$_2$ fragment concentrations on the X axis. Results are representative of 2 independent experiments (n = 2 per condition). By one-way ANOVA: At 10 µg/ml; (C38 IgG, C38 F(ab')$_2$ vs their respective IgG1 controls *P<0.05); at 20 µg/ml; (C10 IgG, C10 F(ab')$_2$, C38 IgG, C38 F(ab')$_2$ vs their respective IgG1 controls ***P<0.001); at 40 µg/ml; (C10 IgG, C10 F(ab')$_2$, C38 IgG, C38 F(ab')$_2$ vs their respective IgG1 controls ***P<0.001).

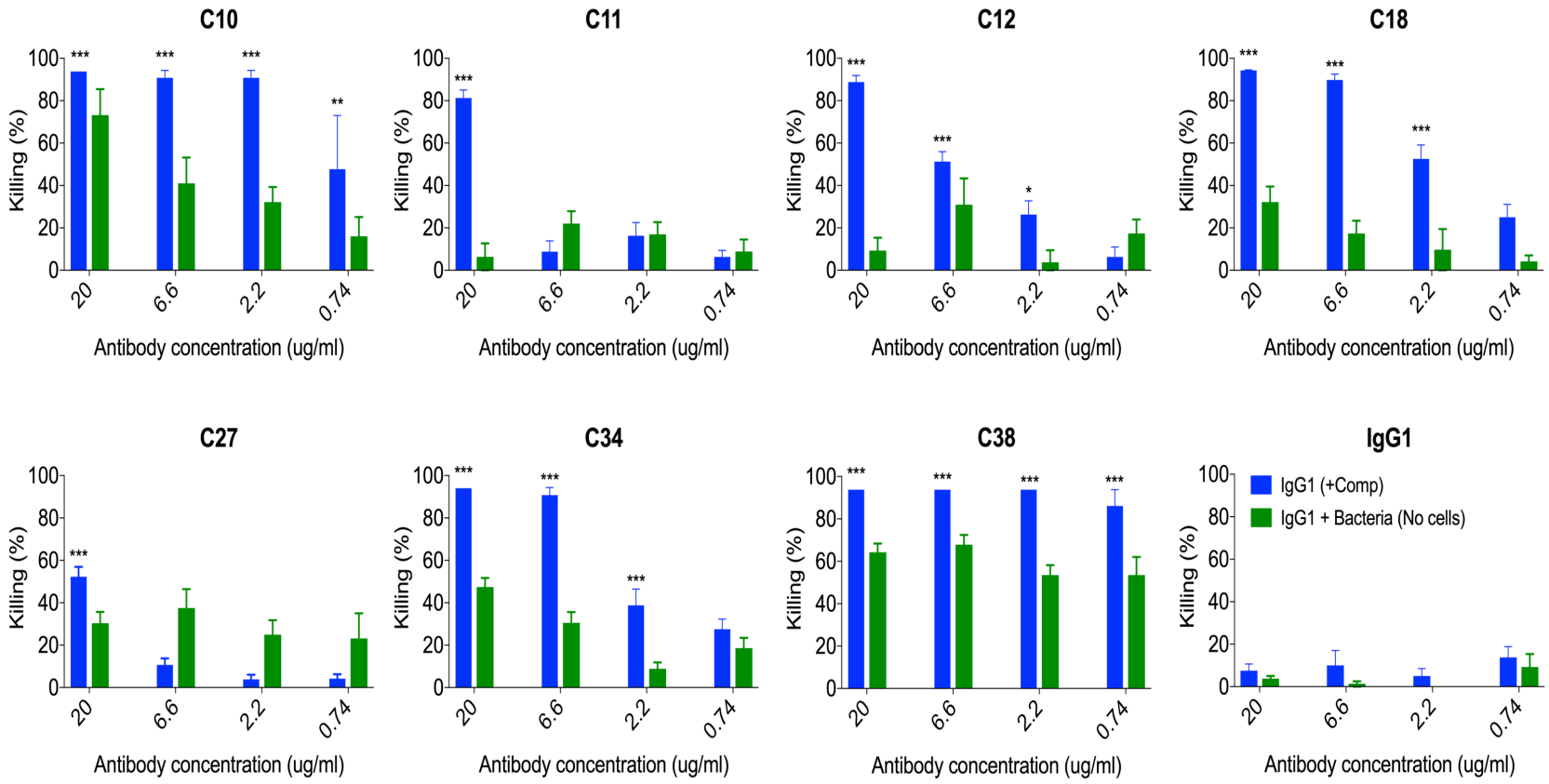

Figure 5: HumAb opsonophagocytic killing of ST3.
HumAbs were tested for their opsonophagocytic killing activity with ST3 (A66) and HL60 cells. Percent killing is shown on the Y axis for the different humAb concentrations shown on the X axis. Results are representative of 2 independent experiments (n = 4 per condition). **P*<0.05, ***P*<0.01, ****P*<0.001 (One-way ANOVA) for humAbs vs IgG1 control.

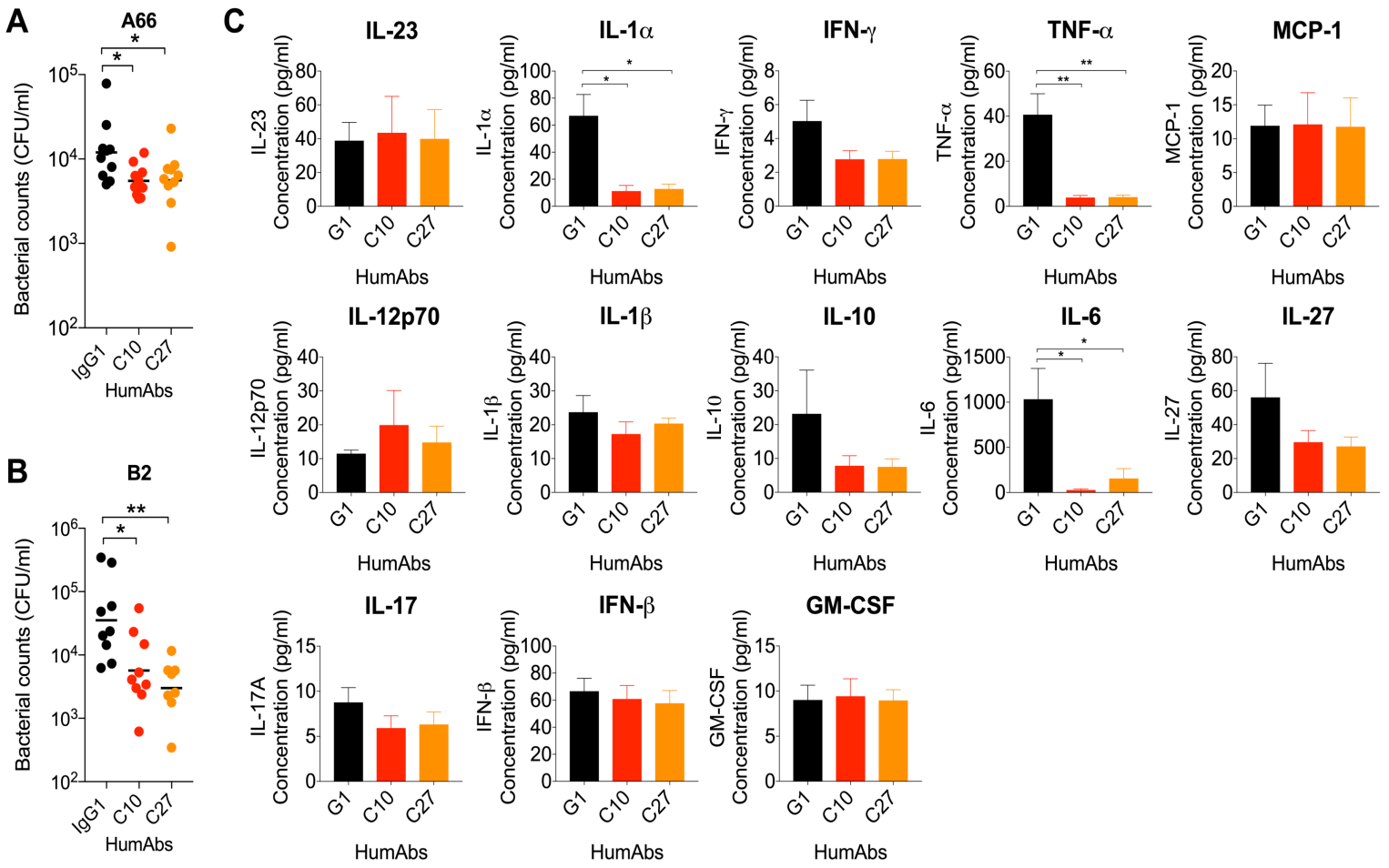

Figure 6: HumAb efficacy against ST3 colonization in C57Bl/6 mice.
HumAbs or a control IgG1 were administered IN in C57Bl/6 mice 2 hrs before IN infection with A) 5 x 10^5 CFU A66 or B) 1 x 10^7 CFU B2. The nasal lavage CFU was enumerated 24 hours (A) or 4 days (B) post infection. CFU are depicted on the Y axis for humAbs shown on the X axis C) Indicated cytokine concentrations via legendplex 4 days after infection of C57Bl/6 mice with 1 x 10^7 CFU B2 (B) are shown on the Y axis for the humAbs on the X axis. Results are representative of 2 independent experiments (n ≥ 5 mice/group). *P<0.05, **P<0.01, ***P<0.001 (One-way ANOVA).

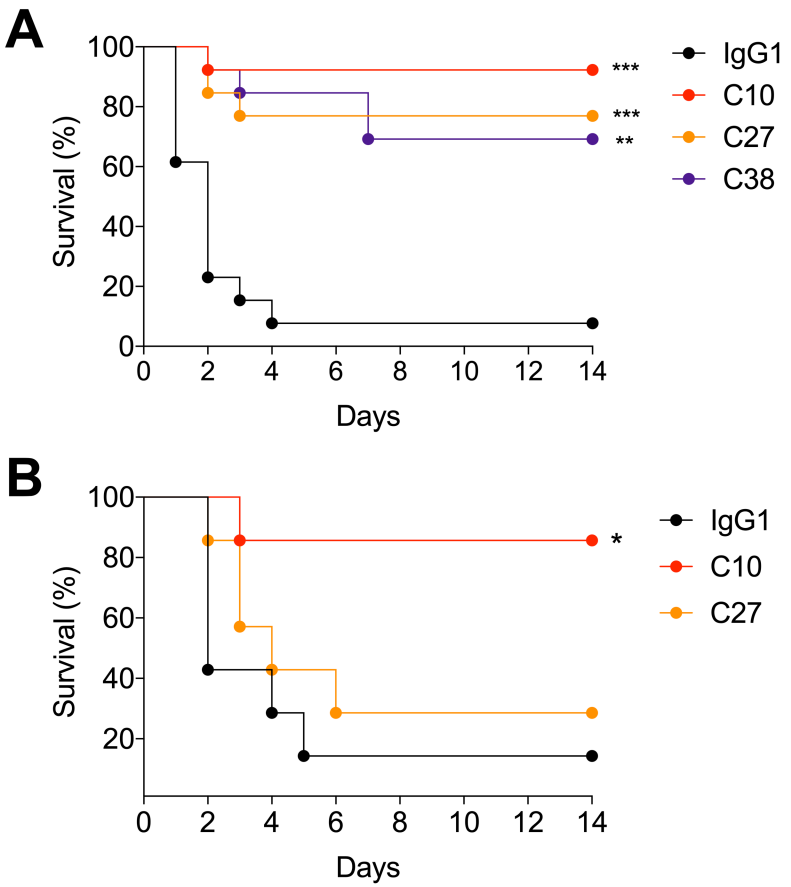

Figure 7: HumAb efficacy against lethal challenge with ST3 strains in C57Bl/6 mice.
A) HumAbs or a control IgG1 were administered IP in C57Bl/6 mice 2 hrs before IP infection with 5x 10^5 CFU A66 and then monitored for survival. B) HumAbs or a control IgG1 were administered IN in C57Bl/6 mice 2 hrs before IN infection with 5 x 10^7 CFU B2 and monitored for survival. All curves show percent survival on the Y axis for the indicated humAbs monitored over 14 days shown on the X axis. Results are representative of 2 independent experiments (n ≥ 7 mice/group). *P<0.05, **P<0.01, ***P<0.001, (Fisher's exact test).

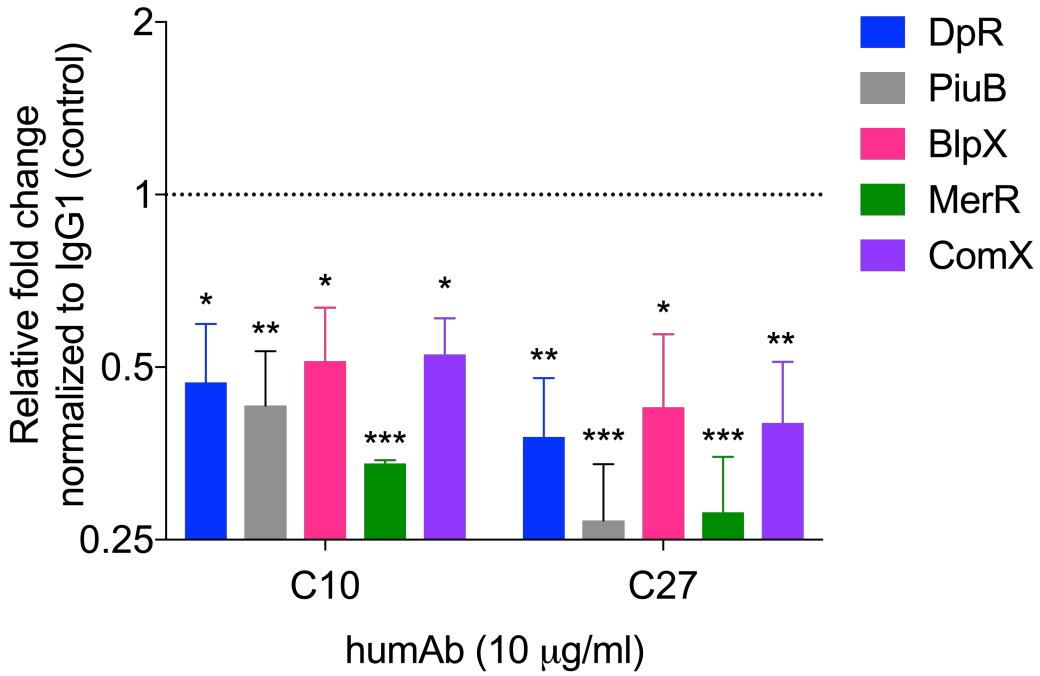

Figure 8: HumAbs mediate changes in expression of bacterial genes related to oxidative stress *in vitro*.
The fold change in expression of the indicated genes in C10 or C27-treated bacteria relative to the control IgG1-treated bacteria was determined by RT-qPCR at 1.5 hours post-humAb addition. Relative expression of genes was determined using the Pfaffl method (55) (fold change is relative to the IgG1 control treated bacteria, expression =1). Data are pooled from 3 independent experiments, 3 samples per condition. **P*<0.05, ***P*<0.01, ****P*<0.001, (One-way ANOVA) C10 or C27 vs IgG1.

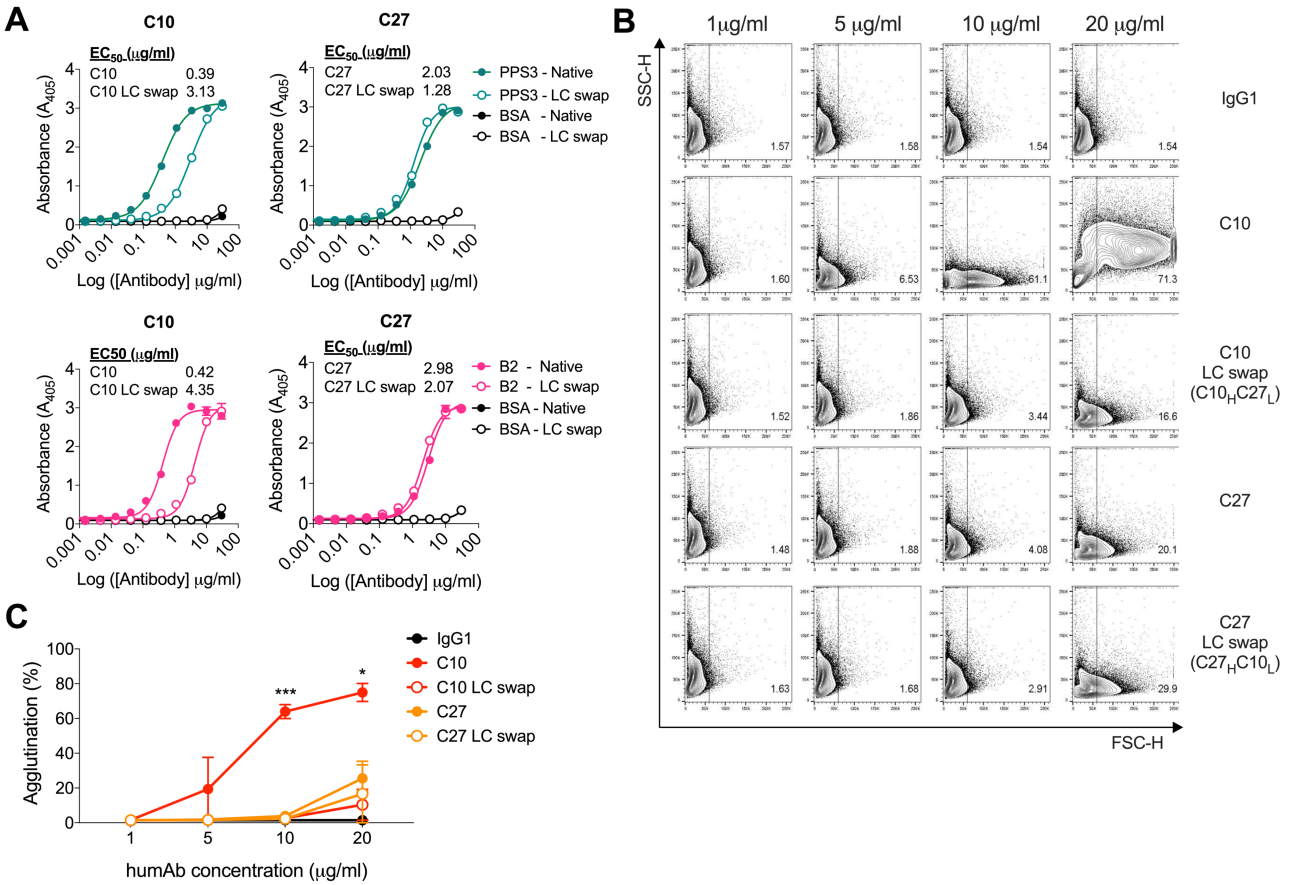

Figure 9: HumAb binding and agglutination of humAbs with light chain swaps.
A) HumAbs (native) with their LC swaps were generated and tested by ELISA for binding reactivity to purified PPS3 and B2. Absorbance at 405 is shown on the Y axis for the humAb concentrations shown on the X axis for each humAb. The numerical half-maximal binding titer (EC_{50}) is depicted on the graph. Results are representative of 3 independent experiments (n = 2). ST3 strain B2 was incubated with increasing concentrations of humAbs (C10, C10 LC swap ($C10_HC27_L$), C27, C27 LC swap ($C27_HC10_L$)) or control IgG1 and analyzed by flow cytometry. B) Representative FACS dot plots showing percentage agglutination of the indicated native humAb or LC swap at various concentrations. C) Line graph depicting percentage agglutination on the Y axis for concentrations of indicated humAbs and LC swaps on the X axis. Results are representative of 2 independent experiments (n = 2 per condition). By one-way ANOVA; at 10ug/ml; (C10 vs IgG1, C10 vs C10 LC swap ($C10_HC27_L$) C10 vs C27, C10 vs C27 LC swap ($C27_HC10_L$) ***P<0.001); at 20ug/ml (C10 vs IgG1, C10 vs C10 LC swap ($C10_HC27_L$), C10 vs C27, C10 vs C27 LC swap ($C27_HC10_L$) *P<0.05

690 **SUPPLEMENTARY MATERIAL LEGENDS:**

691

692 **Table S1:** Primers used for RT-qPCR

693

694 **Figure S1: HumAb binding to ST3 clinical strain B2 by ELISA.**

695 Binding reflected by absorbance at 405 is shown on the Y axis for the humAb concentrations
696 shown on the X axis for each humAb. Results are representative of 3 independent experiments (n
697 = 2). The numerical half-maximal binding titer (EC_{50}) for each humAb is indicated to the right of
698 the panel depicting binding curves of all humAbs.

699

700 **Figure S2: Binding of humAbs to the clinical strain B2 by immunofluorescence.**

701 ST3 clinical strain B2 was incubated with humAbs (20 μg/ml) and antibody binding was
702 detected using IgG conjugated to FITC. Fluorescent images were analysed at 100X
703 magnification and representative of 2 independent experiments (n = 2). Non-specific IgG1 was
704 used as a control. White bar represents 2μM.

705

706 **Figure S3: Heavy chain variable region (V_H) sequences of PPS3-specific humAbs.**

707 HumAb V_H sequences aligned with their germline counterparts based on IMGT/V-QUEST
708 (sequence alignment software). Amino acid changes resulting from somatic mutations are
709 indicated within the sequence alignment.

710

711 **Figure S4: Light chain variable region (V_L) sequences of PPS3-specific humAbs.**

712 HumAb V_L sequences aligned with their germline counterparts based on IMGT/V-QUEST
713 (sequence alignment software). Amino acid changes resulting from somatic mutations are
714 indicated within the sequence alignment.
715
716 **Figure S5: *In vitro* agglutination of a clinical ST3 strain.**
717 HumAbs were tested for their ability to agglutinate a ST3 clinical strain (B2) by flow cytometry.
718 A) Representative FACS dot plots showing the percentage agglutination of all humAbs and
719 control human IgG1 at various concentrations by flow cytometry B) Percentage of agglutination
720 is shown on the Y axis for different humAb concentrations indicated on the X axis. Graph
721 represents data from 2 independent experiments (n = 2 per condition). By one way ANOVA: At
722 5 µg/ml; (C10, C34 & C38 vs IgG1 *P<0.05), at 10 µg/ml; (C10, C12, C34 & C38 vs IgG1
723 ***P<0.001); at 20 µg/ml (C10, C12, C18, C34 & C38 vs IgG1 **P<0.01), at 40 µg/ml (C10,
724 C12, C18, C27 & C38 vs IgG1 **P<0.01).
725
726 **Figure S6: PPS3-PE optimization with ST3 hybridoma cells.**
727 ST3 hybridoma cells were optimized with different concentrations of PPS3-PE with and without
728 the presence of unlabelled PPS3 (25 µg/well). PPS3-PE positive signal was determined by flow
729 cytometry. Histograms represent the following groups; Control (cells with no PPS3-PE) (Red),
730 Pre-incubation (cells pre-incubated with unlabelled PPS3 prior to addition of PPS3-PE) (blue),
731 PPS3-PE (cells incubated only with PPS3-PE) (Orange). Results are representative of 2
732 independent experiments (n = 2).
733
734 **Figure S7: Representative gating strategy to sort for PPS3+ Memory B cells.**

735 PBMCs were collected from patients 7 days following vaccination with pneumococcal vaccines

736 and stained to sort for $CD19^{+}CD27^{+}IgM^{-}IgG^{+}PPS3^{+}$ cells (See Methods for details).

737
738
739